





Article

Integrated Flood Risk Management Approach Using Mesh Grid Stability and Hydrodynamic Model

Azazkhan Pathan ^{1,*} , Komali Kantamaneni ^{2,*} , Prasit Agnihotri ¹, Dhruvesh Patel ³, Saif Said ⁴ 
and Sudhir Kumar Singh ⁵ 

¹ Department of Civil Engineering, Sardar Vallabhbhai National Institute of Technology, Surat 395007, India

² School of Engineering, University of Central Lancashire, Fylde Rd., Preston PR1 2HE, UK

³ Department of Civil Engineering, School of Technology, Pandit Deendayal Energy University, Gandhinagar 382426, India

⁴ Department of Civil Engineering, Z. H. College of Engineering and Technology, Aligarh Muslim University, Aligarh 202002, India

⁵ K. Banerjee Centre of Atmospheric and Ocean Studies, University of Allahabad, Prayagraj 211002, India

* Correspondence: pathanazaz02@gmail.com (A.P.); kkantamaneni@uclan.ac.uk (K.K.)

Abstract: Today, inhabitants residing in floodplains face a serious and perpetual threat of flooding. Flooding causes fatalities and considerable property damage in metropolitan areas. Therefore, robust structural measures need to be adopted to eliminate flood catastrophe. Structural measures in the floodplain are the most promising solutions. However, there are cost-associated factors for proposing a flood retention plan. Navsari city (98.36 km², area extent) of Gujarat was used as a case study to investigate the impact of mesh grid structures (100 m, 90 m, and 50 m) along with structural measures for the preparation of a flood retention plan. The HEC-RAS 2D hydrodynamic model was performed for the Purna River. The output of the model was characterized by four different scenarios: (i) Without weir and levees (WOWL), (ii) With weir (WW), (iii) With levees (WL), and (iv) With weir and levees (WWL). The statistical parameters (R^2 , RMSE, NSE, inundation time, and inundation area) were determined to evaluate model accuracy. The outcome of the model revealed that a 50 m size mesh grid exhibited more accurate results, yielding high NSE and R^2 values (0.982 and 0.9855), a low RMSE value (0.450 m), and a smaller inundation area (114.61 km²). The results further revealed that the WW scenario was the most effective flood retention measure as it delayed the flood water for up to 16 h, and managed the flood with the WOWL case. Moreover, the mean error (WW scenario) estimated from profiles 1 and 2 ranged from (−0.7 to 0.62) and from (−0.1 to 0.02 m), respectively, which were evaluated as very low when compared with other scenarios. The novel scenario-based flood retention plan emphasizing the stability of mesh grid structures using the hydrodynamic model can be applied to any other region around the globe to recommend efficacious structural flood measures for flood decision making systems.

Keywords: flood retention plan; mesh grid stability; with weir 2D hydrodynamic modeling; comparative approach; flood inundation; right and left bank of Purna River; India



Citation: Pathan, A.; Kantamaneni, K.; Agnihotri, P.; Patel, D.; Said, S.; Singh, S.K. Integrated Flood Risk Management Approach Using Mesh Grid Stability and Hydrodynamic Model. *Sustainability* **2022**, *14*, 16401. <https://doi.org/10.3390/su142416401>

Academic Editor: Andrzej Walega

Received: 1 November 2022

Accepted: 2 December 2022

Published: 7 December 2022

Publisher's Note: MDPI stays neutral with regard to jurisdictional claims in published maps and institutional affiliations.



Copyright: © 2022 by the authors. Licensee MDPI, Basel, Switzerland. This article is an open access article distributed under the terms and conditions of the Creative Commons Attribution (CC BY) license (<https://creativecommons.org/licenses/by/4.0/>).

1. Introduction

Floods are a common, recurring, and devastating natural disaster that causes significant property damage and loss of life. Flooding has been the cause of one of the world's most catastrophic climate holocausts and has had enormous socio-economic impacts on all actions and infrastructure inside a flood zone [1,2]. In tropical countries (i.e., India), floods are ubiquitous and frequent. India is among the most flood-prone nations in the world, coming in second after Bangladesh, and accounts for one-fifth of all flood-related deaths worldwide. According to the Disaster Management Authority of India (2008), over 40 million hectares (Mha) out of a total of 329 Mha of geographical area are prone to flooding [3,4]. Flash floods pose a significant risk to humans in many parts of the world [5,6].

Furthermore, flooding is also triggered by flood propagation, frequency, duration, and rising water levels [7,8]. Floods in coastal regions such as Surat city are mainly caused by heavy rainfall, informal settlement along the riverbank, rapid industrialisation and urbanisation, bank erosion, high tides, and a sharp increase in population density [1]. Property damage, environmental quality, economic impact, aesthetic values, and flood uncertainty can be classified as direct, indirect, or uncertainty damages [9,10]. Subsequently, floods affect business, recreational activities, human settlement, industrialization, drinking and irrigation water, and land.

Flood management is essential to reduce the loss of property and the death toll. Due to the rapid urbanization in the city, it is practically impossible to prevent urban flooding [4]. However, significant progress has been made to deter flood damage and flood risk. Flood risk management and assessment are critical steps for flood deluge mapping and identifying flood-prone areas [11,12]. Both structural and non-structural measures can be effective in preventing the loss of property and human life [10,13]. Various studies have been conducted in recent decades on the development of models to predict flooding scenarios and offer appropriate structural and non-structural measures in urban and rural areas [14,15]. Bala et al. [16] instigated flood control measures in and around Dhaka by contracting the flood walls and embankments that protected Dhaka's west city against the riverine flood [17]. Gotoh et al. [18] explored how small-scale reservoirs were used as an effective flood-control tool in various regions of Japan in recent decades. Jayswal et al. [19] adopted the Terramesh wall as a flood control structure that does not need skilled labour and has the flexibility to absorb variable ground settlements without jeopardizing structural integrity.

Interestingly, hydrodynamic models for 1D, 2D, and 1D/2D combined hydrodynamic modeling exist widely these days due to the ease of the simulation process of various flood scenarios [9,20,21]. The Hydrologic Engineering Centre River Analysis System (HEC-RAS) is the most extensively used model that has been established for a variety of computations of steady and unsteady flow [22]. Zhang et al. [23] employed the HEC-RAS to analyse flood risks in the Pearl River Delta and suggest appropriate mitigation measures for the North Pearl River Levee System (NPRLS) of Guangdong State, China. Patel et al. [24] used a 1D/2D coupled hydrodynamic HEC-RAS model to replicate the flood event of 2006, with and without bank protection works, in low-lying areas of Surat, India. Fadillah et al. [25] have used HEC-RAS for hydraulic analysis on the Ciliwung River and recommended the dam on the upstream side of the river. Moreover, various studies have been carried out using HEC-RAS 1D and 2D for structural flood control measures in order to palliate extreme flood events [26–28]. However, very few researchers have accomplished a mesh size-based flood inundation modeling approach using the 2D HEC-RAS model [29–31].

The city of Navsari in Gujarat, which is located along the Arabian coast, has significant industrialization and urbanization growth. Consequently, the population of the city has increased enormously (Census 2011–2021). The city witnessed a flash flood on 14 July 2022, which inundated and flooded various areas, including Viraval, Jalalpore, and Virawadi. Due to continuous rains, the Purna River surpassed the alert level by five feet. While thousands of people were evacuated and relocated to safer areas, the flooding severely affected low-lying areas of the city. There has not been much flood assessment research carried out for the city of Navsari in recent years. However, Pathan and Agnihotri [7] have evaluated the application of the newly released HEC-RAS version for 1D hydrodynamic modeling to assess the flood depth, velocity, and water surface elevation downstream of the Purna river, Navsari city. In addition, they have used the 2D HEC-RAS model and identified the efficacy of tide waves on hydrodynamics [32].

In view of the aforementioned flood causalities in Navsari and the lack of studies in the agitated domain, it is essential to develop appropriate and effective flood retention plans to alleviate the flood and reduce vulnerability. However, in the existing literature, the selection of a suitable mesh grid for the development of various scenario-based flood retention plans is still imprecise. As a result, the Purna River in Navsari City has been

chosen as a case study to demonstrate an approach to reduce uncertainty and fill the research gap in selecting the appropriate mesh grid structure for the scenario-based flood retention plan. Furthermore, using four different scenario-based flood decision-making systems, this study presents a novel case for implementing flood control and retention measures. In addition, the study intends to compare the results of a hydrodynamic model scenario with performance evaluation methods. This approach will help to improve the efficiency of flood mitigation and countermeasures while also reducing flood damage. The study considers four structural flood control scenarios (i.e., WOWL, WW, WL, and WWL) in the 2D HEC-RAS model. The outcome of the work will be utilized by local, as well as worldwide, government and disaster management authorities to prepare a cost-effective flood retention plan for flood mitigation planning.

2. Study Area

Navsari is a renowned tourist attraction in Gujarat, a coastal state in India (Figure 1). It is also known as Surat's twin city. The city of Navsari has a longitude of $72^{\circ}42''$ – $73^{\circ}30''$ E and a latitude of $20^{\circ}32''$ – $21^{\circ}05''$ N, and a total area of 2211.97 km² [7]. The Purna River flows through the city, with a total catchment area of 2373 km². Of this, 53 km² is covered by Gujarat state, and 58 km² is covered by Maharashtra state. The city has a population of 1.71 million people according to the 2011 Census of India. The city has warm weather from October to May, with an average yearly rainfall of 122 cm from June to September during the southwest monsoon period [32]. The lowest and highest daily average temperatures range from 17 °C to 40 °C. The city has a national literacy rate of 88%, which is higher than the national average of 74%.

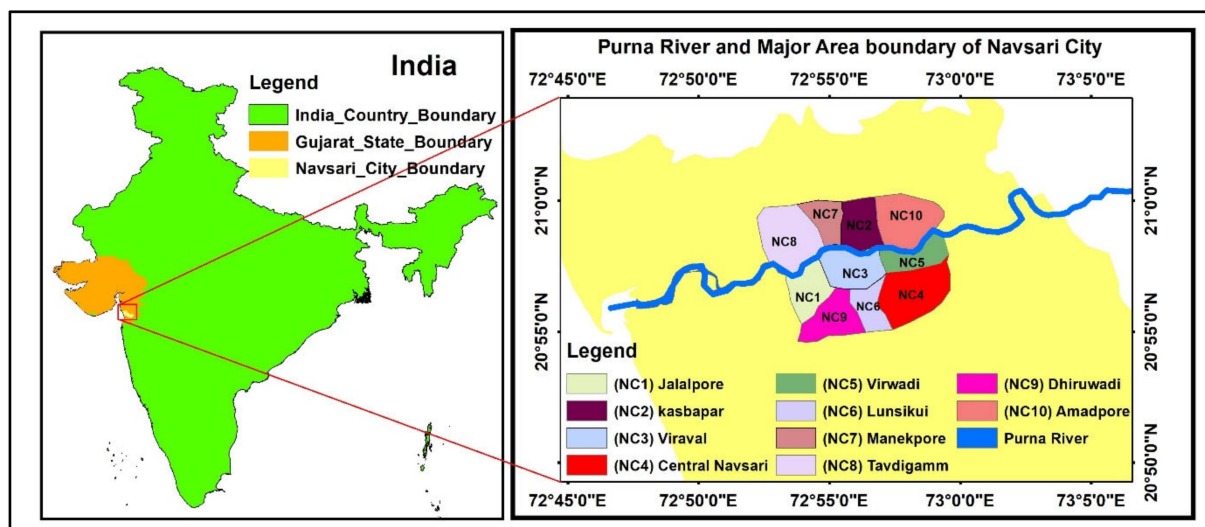


Figure 1. Location map of the study area.

Figure 2 provides a view of the city's devastating flooding, which occurred on 4 August 2004. Global warming, uneven rainfall patterns, rapid urbanization, industrial development, and coastal changes are the primary reasons for the flooding events in the city.

The entire study area (i.e., Navsari city) was divided into 10 sub-areas based on the town planning scheme and population density. Hence, the impact of flood control measures, such as vegetation and the dams/reservoirs/weirs surrounding the main area of Navsari city, could be assessed. The divided sub-areas were identified as Jalalpore, Kasbapore, Viraval, Central Navsari, Viravadi, Lunsikui, Manekpore, Tavdigamm, Dhiruwadi, and Amadpore, and designated from NC1 to NC10, respectively, and the areal extent of the sub-areas was evaluated (Table 1).



Figure 2. Flooded areas in Navsari city during 4 August 2004 floods: (a) Viraval (NC3), (b) Jalalpore (NC1), (c) Lunsikui (NC6), and (d) Manekpore (NC7).

Table 1. Identified 10 sub-areas within Navsari city and their respective areal coverage.

Sub Areas	Designate	Total Area (km ²)	Total Area (%)
Jalalpore	NC1	8.0	8.13
Kasbapore	NC2	8.4	8.54
Viraval	NC3	10.4	10.57
Central Navsari	NC4	15.2	15.45
Virawadi	NC5	7.0	7.11
Lunsikui	NC6	5.75	5.84
Manekpore	NC7	6.0	6.10
Tavdigamm	NC8	14.7	14.97
Dhiruwadi	NC9	9.66	9.82
Amadpore	NC10	13.25	13.47
Total Area		98.36	

Data

Open-source SRTM 30 m resolution DEM was used for 2D HEC-RAS modeling (<https://earthexplorer.usgs.gov/>, accessed on 12 May 2019). The soil data were extracted from the National Bureau of Soil Survey and Land Use Planning (NBSS and LUP-2022), Maharashtra, India. Land use and land cover classification were mapped using Landsat 8 satellite images -2019. The discharge and water level data were obtained from Navsari Irrigation Circle (NIC) and the Central Water Commission (CWC), India.

3. Material and Methods

Many researchers have assessed 2D hydrodynamic modeling to identify flood inundation and its extent with open-source hydrodynamic models [1,4,6,7]. Furthermore, flood control measures have also been proposed in order to reduce the severity of floods [3,6,10,33,34]. However, scenario-based structure flood control measures and the effect of mesh grid stability on flood inundation have not yet been explored. Therefore, to fill this research methodology gap, the present study evaluated flood scenarios using the HEC-RAS 2D hydrodynamic model, and the grid structure model.

Navsari city experienced disastrous floods in the years 1968 and 2004. Very few flood assessment studies have explored this area. The city is affected by floods every year during the monsoon season and it leads to losses in properties and lives. The effect of mesh grid stability is influential in hydrodynamic modeling. Therefore, to alleviate the extent of flooding and the consequential damages caused by frequent floods in the city, the flood of the 4 August 2004 was used as a standard case (WOWL) and three scenarios (i.e., WW,

WL, and WWL) were simulated in order to evaluate a comparative assessment for the most suitable structural flood control measures. The most appropriate mesh grid stability was also evaluated in the context of a scenario-based flood retention plan for the study area. The integrated flood risk management of mesh grid stability and 2D hydrodynamic modeling is depicted in Figure 3.

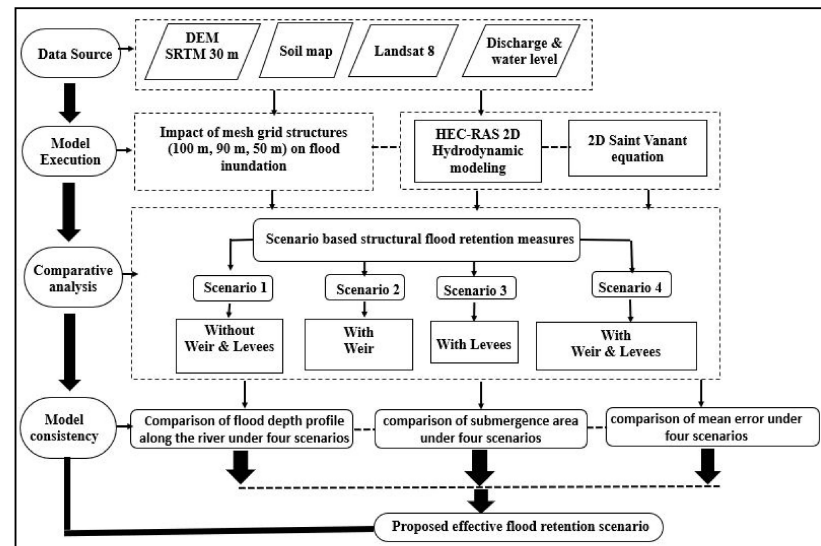


Figure 3. Stepwise procedure adopted for flood control measures.

3.1. 2D HEC-RAS Hydrodynamic Flood Modeling

This study used the 2D HEC-RAS model to simulate four scenarios (i.e., WOWL, WW, WL, and WWL) to visualize the extent of the flood in order to devise structural flood control measures and flood management strategies for the city. The 4 August 2004 flood event was executed to simulate the model. Furthermore, the unsteady flow was simulated. Subsequently, flood hydrograph and normal depth were used as upstream and downstream boundary conditions, respectively. The new HEC-RAS version 5.0.7, designed by the USACE, was used to simulate the flood event. The 2D Saint-Venant equations or the 2D diffusion wave equation were solved by the HEC-RAS, version 5 [1,20,32,35].

$$\frac{\partial \zeta}{\partial t} + \frac{\partial p}{\partial x} + \frac{\partial q}{\partial y} = 0 \quad (1)$$

$$\frac{\partial p}{\partial t} + \frac{\partial}{\partial x} \left(\frac{p^2}{h} \right) + \frac{\partial}{\partial y} \left(\frac{pq}{h} \right) = -\frac{n^2 pg \sqrt{p^2 + q^2}}{h^2} - gh \frac{\partial \zeta}{\partial x} + pf + \frac{\partial}{\partial x} (h\tau_{xx}) + \frac{\partial}{\partial y} (h\tau_{xy}) \quad (2)$$

$$\frac{\partial q}{\partial t} + \frac{\partial}{\partial y} \left(\frac{q^2}{h} \right) + \frac{\partial}{\partial x} \left(\frac{pq}{h} \right) = -\frac{n^2 qg \sqrt{p^2 + q^2}}{h^2} - gh \frac{\partial \zeta}{\partial y} + qf + \frac{\partial}{\partial y} (h\tau_{yy}) + \frac{\partial}{\partial x} (h\tau_{xy}) \quad (3)$$

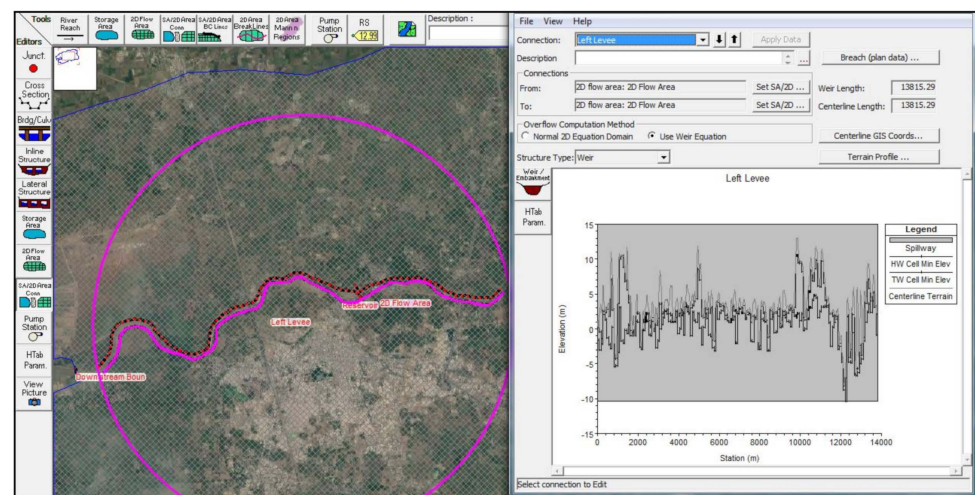
where h = depth of water (m); p , q = specific flow in the x and y direction $\text{m}^2 \text{s}^{-1}$; ζ = surface elevation (m); g = gravitational acceleration (m s^{-2}); n = Manning resistance; ρ = water density (kg m^{-3}); τ_{xx} , τ_{xy} , τ_{yy} = the components of effective shear stress; and ' f ' is the Coriolis (s^{-1}) [20,24,32].

3.2. Analysis of Mesh Grid Structures for Flood Risk Assessment

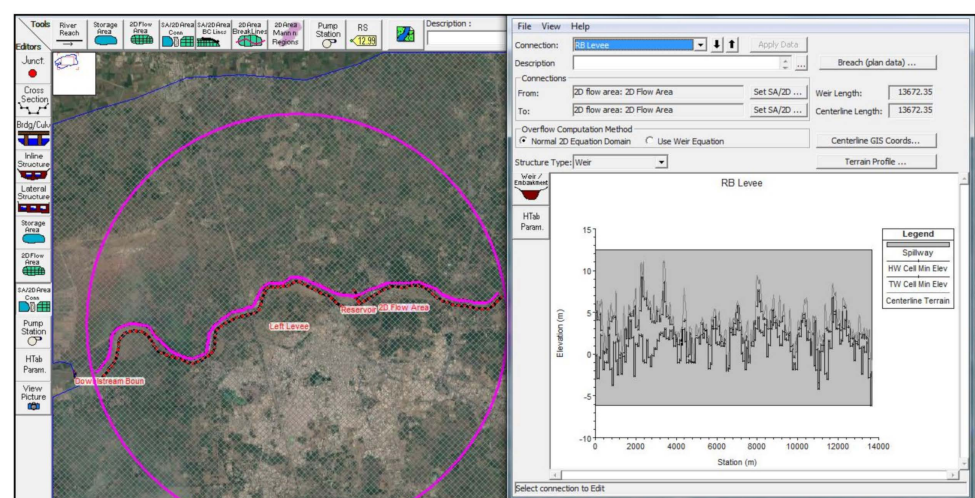
The impact of altered mesh grid structures (100, 90, and 50 m) on flood inundation was assessed, and the 4 August 2004 flooding event was simulated in the 2D HEC-RAS model for the study area. The assessment of diverse mesh grid structures aims to achieve a higher level of precision in the shortest amount of computational time. Even though higher resolution enables speedier simulations, it comes at the expense of accuracy. The terrain will be better illustrated but it will require more computational time [36]. The HEC-RAS 2D geometric data editor window has a feature which draws a polygon to define the study

area's 2D flow area. A total of three mesh grid structures (100×100 m, 90×90 m, and 50×50 m) at the spacing of the computational points were evaluated to analyze the impact of these mesh grid structures on the run time and performance of the model. The average grid sizes and the number of grid cells of the aforesaid grid structures were obtained as (average cell size = $10,066.39 \text{ m}^2$, 48,026), (average cell size = 8147.91 m^2 , 59,339), and (average cell size = 2512.44 m^2 , 192,437).

A four-point implicit finite volume algorithm was used to solve the selected model. The unstructured mesh was provided with a conventional method in the finite volume approach, which calculates the mean integral of the reference volume. For each computational cell face, relationships between elevation-hydraulic properties as well as elevation volume were estimated. Before the calculation began, hydraulic property tables were obtained. In the second phase, the SA/2D area connection tool was used to locate the levees and the reservoir/dam inside the 2D flow areas (Figure 4). The long levees (12,122 and 12,396 m) were generated on the left and right banks of the Purna River adjoining Navsari city (Figure 4a,b). In addition, the HEC-RAS geometry of the reservoir/dam near the Viraval area, Navsari is illustrated in Figure 4c.

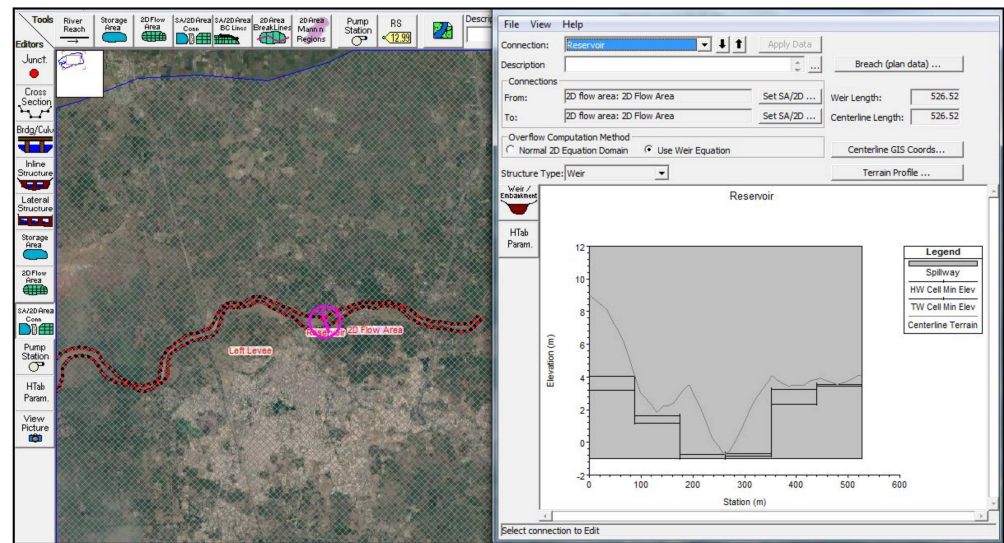


(a)



(b)

Figure 4. Cont.



(c)

Figure 4. (a) HEC-RAS geometry with proposed levees structures on the left bank of the Purna River, Navsari; (b) HEC-RAS geometry with proposed levees structures on the right bank of the Purna River, Navsari; and (c) HEC-RAS geometry with proposed weir near Viraval, Navsari.

Since, a major part of the study area is comprised of silty clay soil, the Manning roughness coefficient was selected as 0.035 in the model simulation [37,38]. Lastly, the time steps were calculated in conformity with the Courant–Friedrichs–Lewy condition to confirm the constancy of the model [35].

$$C = \frac{V\Delta T}{\Delta X} \leq 1 \text{ (with maximum } C = 3) \quad (4)$$

$$\Delta T \leq \frac{\Delta X}{V} \text{ (with } C = 1) \quad (5)$$

where C = Courant Number; v = Flood wave velocity ms^{-1} ; ΔT = Computational time step (s); and Δx = Average cell size (m) [32,35].

4. Results

4.1. Structural Flood Control Measures Using HEC-RAS 2D Hydrodynamic Modeling

Flood protection work is essential considering the properties and lives at stake. In the current study, the whole study area was categorized into 10 sub-areas (i.e., NC1 to NC10), and the flood progress in every sub-area was examined. NC1, NC3, NC4, NC6, and NC9 are the important areas of Navsari city where the maximum urbanization has taken place. The main objective of the present study was to analyse, among four scenarios (i.e., WOWL, WW, WL, and WWL), which scenario is most suitable to subside the flood. WOWL is the standard scenario used to compare with the three differing scenarios, i.e., WW, WL, and WWL, considered in the present study. Therefore, in this study, three different approaches were considered for determining the most efficacious structural flood control measures.

1. The first approach was to compare the flood depth in all possible flood scenarios along the two profiles that surround the flood plain. The profile that had the least flood depth in the given scenario would be best for flood protection.
2. The second approach was to compare submergence areas under the aforementioned scenarios, with the scenario with the smallest submergence area being the optimal one.
3. The third approach was to compare the mean error for the above scenarios, with the best scenario being the one with the lowest error.

Simulated 2004 flood inundation maps of Navsari city corresponding to the arrival times for WOWL, WW, WL, and WWL are shown in Figures 5–8. The areas under inundation (in Km^2) corresponding to the arrival time with all four scenarios are illustrated in Table 2.

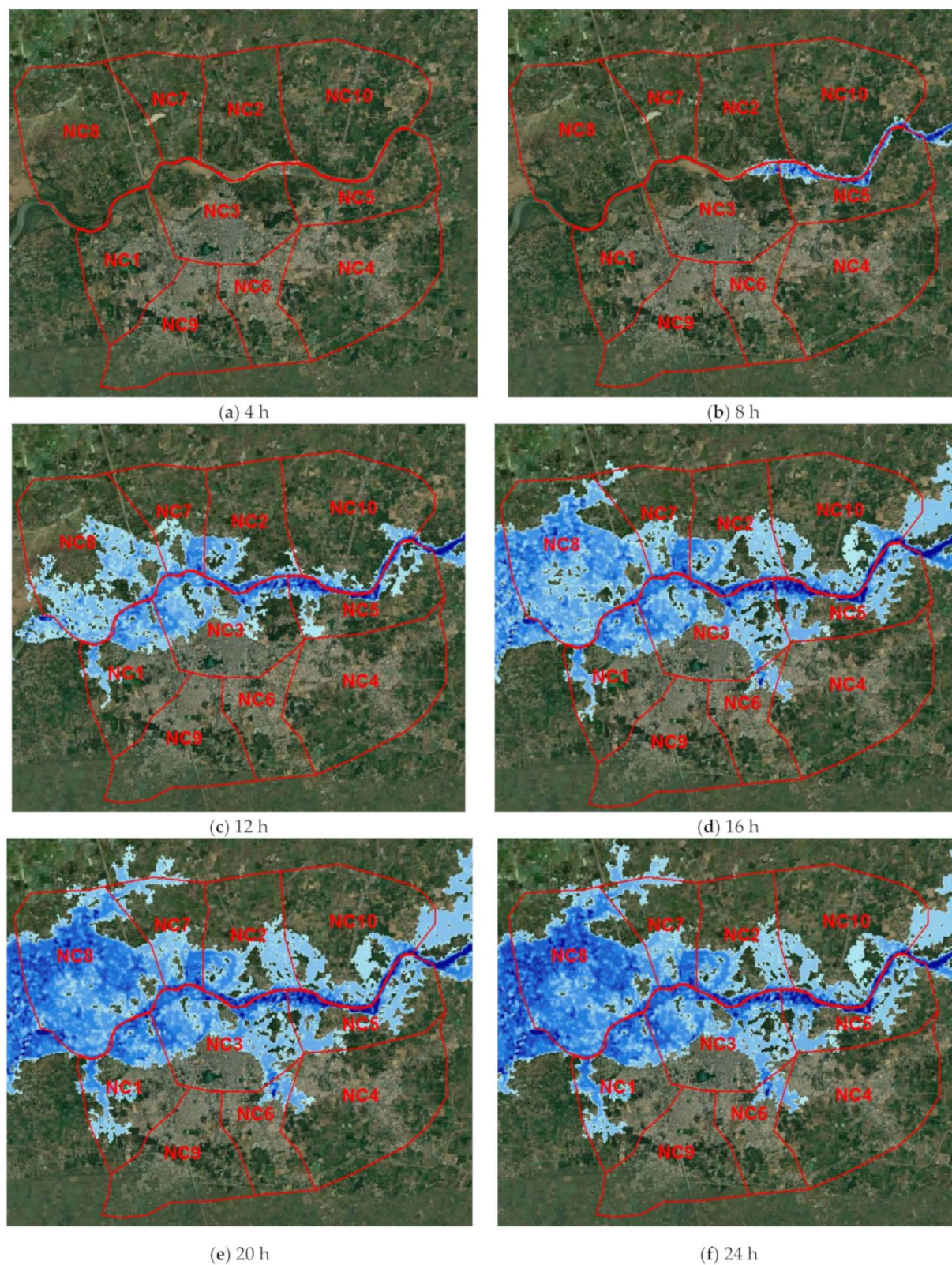


Figure 5. Flood inundation map of Navsari city for the 2004 discharge without weir and levees (WOWL).

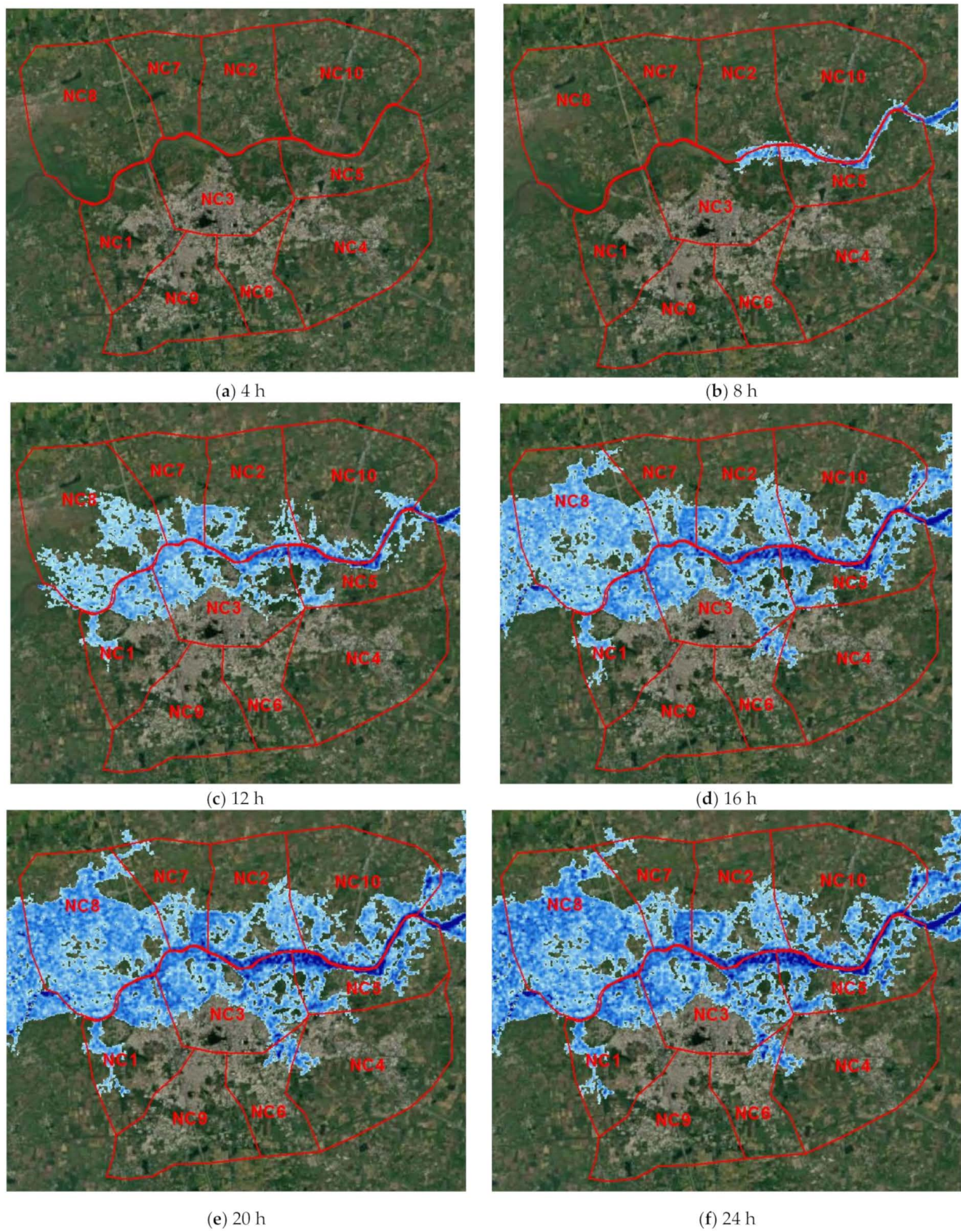


Figure 6. Flood inundation map of Navsari city for the 2004 discharge from with weir at Viraval (WW).

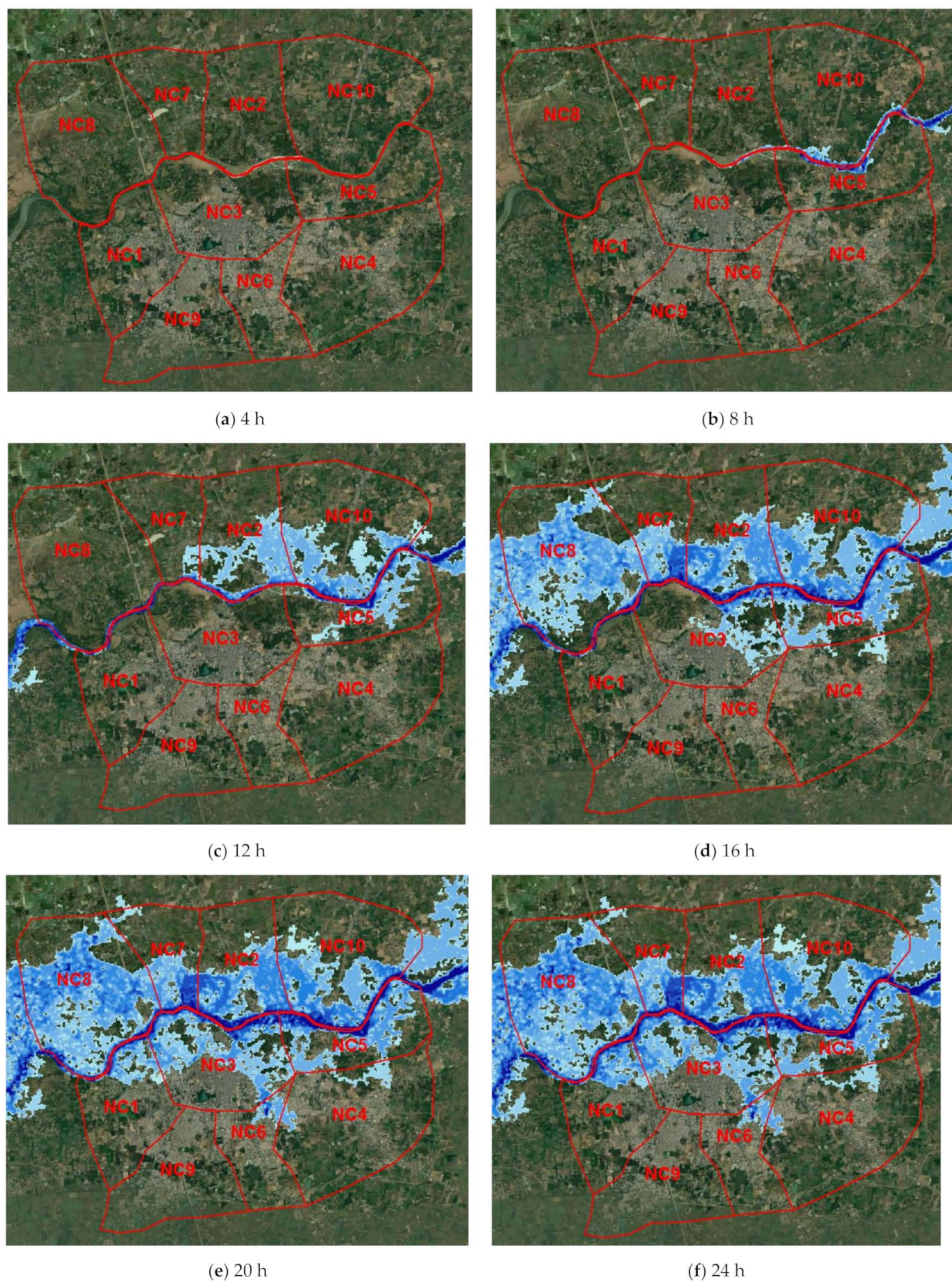


Figure 7. Flood inundation map of Navsari city for the 2004 discharge with levees both side (L.B and R.B) (WL).

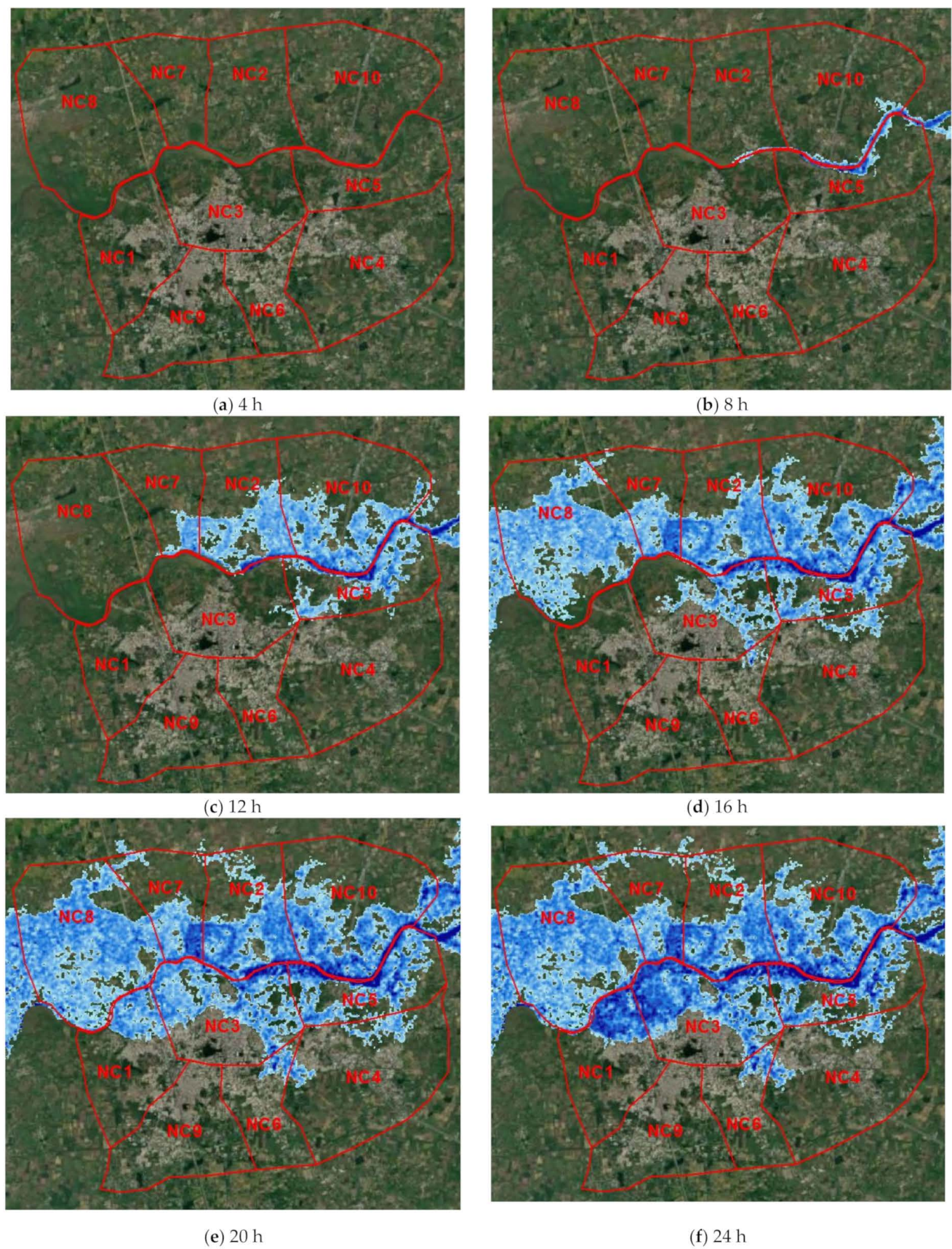


Figure 8. Flood inundation map of Navsari city for the 2004 discharge with weir and levees on both side (L.B and R.B) (WWL).

Table 2. Areal extent of flood inundation within 10 identified sub areas in Navsari city evaluated from four scenarios (i.e., WOWL, WW, WL, and WWL).

Location			NC1	NC2	NC3	NC4	NC5	NC6	NC7	NC8	NC9	NC10
Arrival Time (Hours)	Scenarios	Inundation Area										
8	WOWL	km ²	0.37	0.07	0.00	0.00	0.00	0.00	0.90	0.00	0.00	0.00
		%	4.63	0.79	0.00	0.00	0.00	0.00	14.93	0.00	0.00	0.00
	WW	km ²	2.12	1.86	4.02	0.00	2.05	0.00	1.02	4.14	0.00	1.30
		%	26.45	22.09	38.65	0.00	29.22	0.00	17.05	28.13	0.00	9.83
	WL	km ²	3.83	2.81	0.00	0.36	0.00	0.00	0.29	2.25	0.00	0.22
		%	47.86	33.51	0.00	2.37	0.00	0.00	4.86	15.28	0.00	1.63
	WWL	km ²	0.00	0.08	0.05	0.00	0.67	0.00	0.00	0.00	0.00	0.53
		%	0.00	1.00	0.51	0.00	9.54	0.00	0.00	0.00	0.00	4.01
12	WOWL	km ²	1.07	1.68	1.27	5.43	2.30	0.00	2.00	0.00	0.00	0.00
		%	13.38	20.00	12.21	35.74	32.92	0.00	33.33	0.00	0.00	0.00
	WW	km ²	2.12	1.86	4.02	0.00	2.05	0.00	1.02	4.14	0.00	1.30
		%	26.45	22.09	38.65	0.00	29.22	0.00	17.05	28.13	0.00	9.83
	WL	km ²	3.83	2.81	0.00	0.36	0.00	0.00	0.29	2.25	0.00	0.22
		%	47.86	33.51	0.00	2.37	0.00	0.00	4.86	15.28	0.00	1.63
	WWL	km ²	0.00	0.08	0.05	0.00	0.67	0.00	0.00	0.00	0.00	0.53
		%	0.00	1.00	0.51	0.00	9.54	0.00	0.00	0.00	0.00	4.01
16	WOWL	km ²	3.37	3.07	1.82	10.96	2.57	0.59	3.25	0.23	0.00	0.42
		%	42.10	36.55	17.50	72.11	36.71	10.26	54.15	1.53	0.00	3.14
	WW	km ²	2.46	3.25	5.57	0.27	3.17	0.47	1.60	10.12	0.00	3.32
		%	30.78	38.67	53.52	1.78	45.26	8.13	26.65	68.86	0.00	25.06
	WL	km ²	5.26	4.13	0.00	2.04	0.37	0.00	2.21	3.72	0.00	0.22
		%	65.78	49.18	0.00	13.45	5.34	0.00	36.76	25.30	0.00	1.65
	WWL	km ²	0.00	4.37	2.64	0.68	3.99	0.16	2.06	9.25	0.00	5.95
		%	0.00	52.02	25.38	4.47	57.00	2.78	34.33	62.93	0.00	44.91
20	WOWL	km ²	3.52	3.29	2.58	12.26	3.32	0.60	3.36	0.33	0.00	0.52
		%	44.05	39.17	24.82	80.66	47.43	10.43	55.95	2.24	0.00	3.92
	WW	km ²	2.63	3.37	5.81	0.35	3.32	0.50	1.83	10.83	0.00	3.83
		%	32.89	40.16	55.88	2.33	47.44	8.74	30.42	73.68	0.00	28.90
	WL	km ²	5.56	4.20	0.46	2.17	0.75	0.56	4.91	3.82	0.00	1.42
		%	69.56	50.00	4.46	14.27	10.77	9.74	81.87	26.00	0.00	10.68
	WWL	km ²	1.69	4.85	5.53	1.11	4.19	0.52	2.30	10.70	0.00	6.04
		%	21.13	57.74	53.17	7.30	59.86	9.04	38.33	72.79	0.00	45.58
24	WOWL	km ²	3.27	3.21	2.67	12.41	3.44	0.61	3.15	0.30	0.00	0.50
		%	40.84	38.21	25.67	81.64	49.19	10.61	52.50	2.07	0.00	3.74
	WW	km ²	2.65	3.22	5.61	0.33	3.11	0.48	1.80	10.82	0.00	3.47
		%	33.11	38.32	53.95	2.14	44.43	8.32	29.96	73.62	0.00	26.19
	WL	km ²	5.57	4.18	0.47	2.17	0.75	0.58	5.07	3.79	0.00	1.63
		%	69.63	49.72	4.51	14.25	10.77	10.09	84.44	25.80	0.00	12.28
	WWL	km ²	2.06	4.74	6.38	1.09	4.04	0.56	2.39	10.66	0.00	5.85
		%	25.75	56.43	61.35	7.17	57.71	9.74	39.83	72.52	0.00	44.15

4.1.1. Comparison of Flood Depth Profile along the River under Four Scenarios

Two profile lines were drawn across the flood plain to observe the flood depth profile in each scenario. As shown in Figure 9, profile 1 and profile 2 are placed on the right and left sides of the river, respectively. In the first scenario, (WOWL), which was taken as a standard scenario, it was observed that at the beginning of the flood, there was a significant amount of water depth ranging from 0.5–3.5 m in the first 8 h, along with all sub-areas (i.e., NC1 to NC10) of the city. However, there was no flood in the other three scenarios (WW, WL, and WWL) (Figure 10a). As soon as the arrival time increased from the 8th to the 12th hour, there was a significant increase in the flood depth in all four scenarios. However,

there was less flood depth observed in the cases of WW, WL, and WWL when compared with WOWL. At the 12th hour, the most effective flood protection approach was WW and WL for the NC8 to NC2 sub-areas, in which the flood depth varied between 2.2 and 4.2 m. However, WW also showed an effective approach in the two sub-areas, NC2 and NC10, in profile 1, which showed almost zero depth.

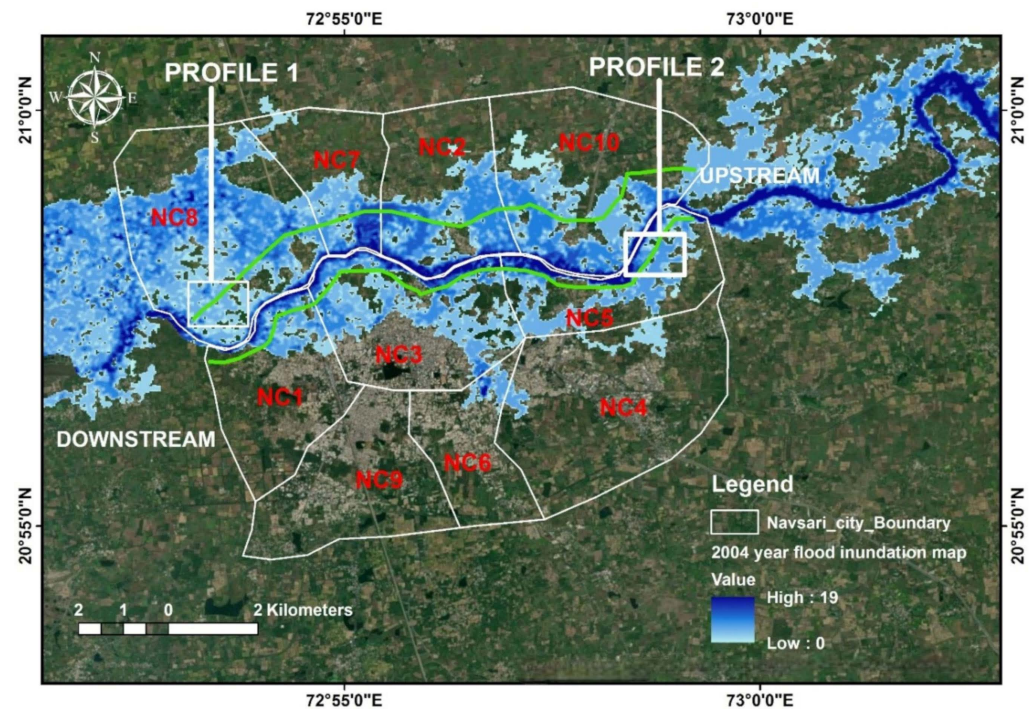
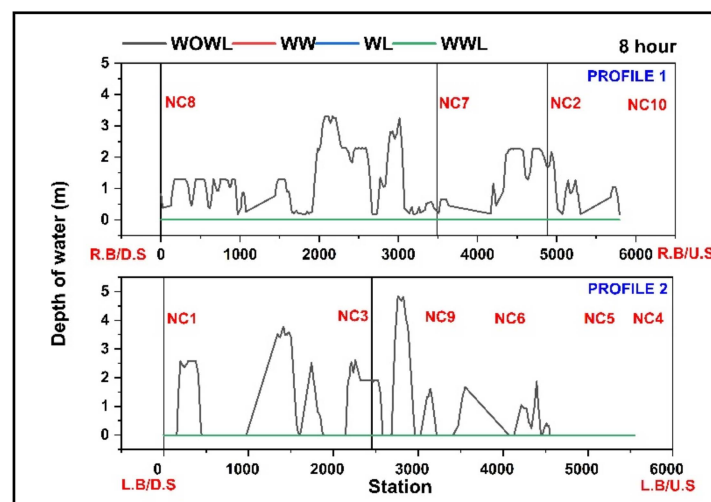
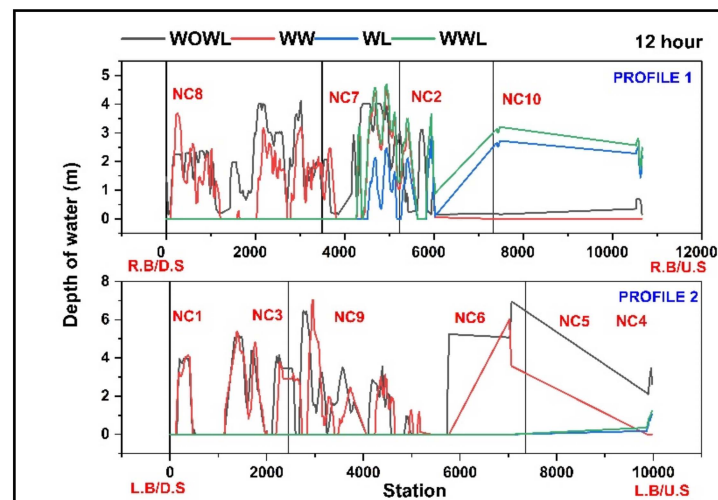


Figure 9. Profile lines (1) From downstream to upstream on right bank of Purna river; and profile line (2) From downstream to upstream on left bank of Purna river.

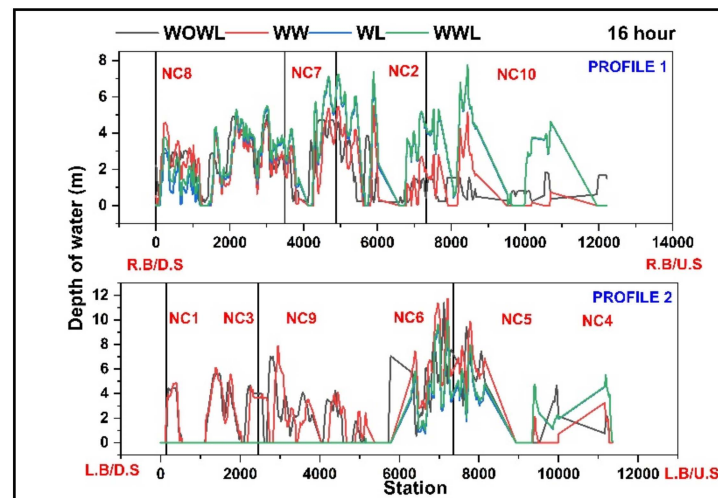


(a)

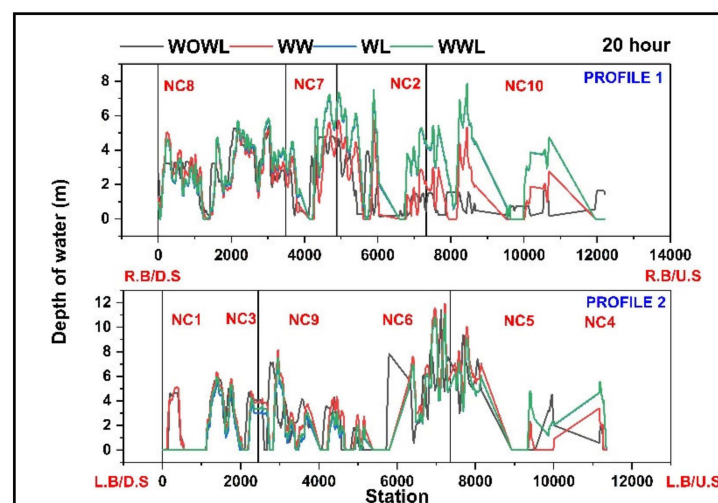
Figure 10. Cont.



(b)

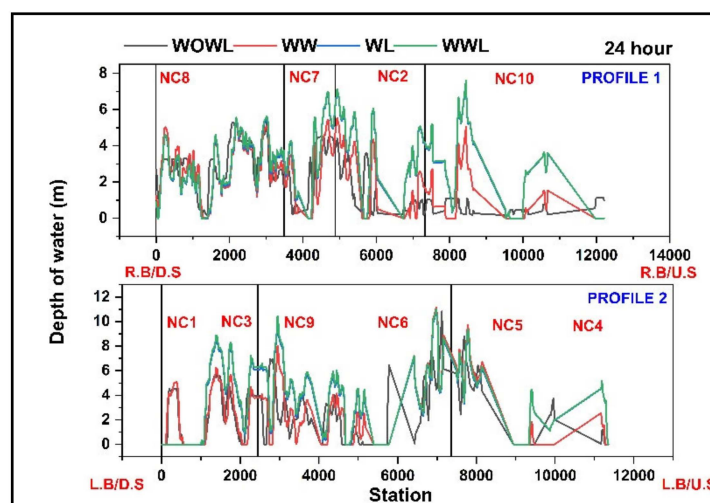


(c)



(d)

Figure 10. Cont.



(e)

Figure 10. Water level profiles along the Purna River for the 2004 flood; (a) 8 h; (b) 12 h; (c) 16 h; (d) 20 h; and (e) 24 h.

Moreover, in profile 2 the WWL showed to be an effective approach (depth variation between 0.5 and 4.5 m) and the WW was observed to be the worst approach (depth variation between 1 and 7 m) (Figure 10b). Therefore, it can be concluded that at the 12th hour, WWL was the most effective measure to counter the flood. At the 16th hour, the WW scenario was proven more effective in profile 1 and it was still an effective measure compared with the standard scenario (WOWL) for the sub-areas NC8, NC7, NC2, and NC10 (depth variation between 0.5 and 5 m). Simultaneously, in profile 2, the WWL approach was shown as an effective countermeasure for the sub-areas NC1, NC3, and NC9 (depth variation up to 6.9 m), for NC6 (up to 10 m) and for NC5, NC4 (depth variation between 1 to 5 m) (Figure 10c). Of course, greater variation was observed in the different approaches for counter-flood measures at the 16th hour because the upstream flood had influenced the flooding effect towards the downstream.

Therefore, at present, WW and WWL cases can be considered the most effective flood retention approaches. All four scenarios depict similar results at the 20th and 24th hour arrival times. WW was an effective counter measure for preventing the flood for profile 1, in which the flood depth was recorded up to 4.9 m, whereas in profile 2, for the sub-areas NC1, NC3, and NC9, it varied between 3.9 and 7 m, and for NC5 and NC4, it appeared to be 2 m. However, the flood water was observed to be higher (up to 11.5 m) in NC6. In addition, it was observed up to 10.5 m in the case of the 24th hour (Figure 10d,e). It should be noted that the WW scenario showed a flood level almost equal with the standard scenario (WOWL). However, it delayed the flood by almost 12 h. Therefore, the WW scenario revealed an effective flood retention approach that can be used for structural flood protection measures in Navsari city.

4.1.2. Comparison of Submergence Area under Four Scenarios

A comparatively lower level of inundation, ranging from 0 to 0.66 km², was observed at the 8th hour in the cases of the WOWL and WWL scenarios, while a considerably higher level of inundation occurred (0.55 to 4.13 km²) in the cases of WW and WL scenarios. Considering an individual area of the city, i.e., NC1, the maximum amount of inundation took place after the 20th hour, which was around 5.56 km² (69.5%) under the WL scenario. The least amount of inundation was observed for the WWL scenario, which was almost zero up to the 16th hour. After the 16th hour, inundation increased slightly up to 2.06 km² (25.75%). For NC2, the WWL scenario was proven to be more effective up to the 12th hour as it showed an inundation of 0.08 km² (0.95%), whereas the WW scenario was observed to

be less effective as it showed an inundation of 3.21 km² (38.21%). Maximum inundation was observed in the case of WWL, which covered 4.74 km² (56.42%) between the 16th and 24th hours. Inundation increased because, as the volume continues to rise in a body of water, after a certain time, i.e., the 16th hour, the body of water overfills and water starts inundating the area. The WL scenario was most effective for the sub-area NC3 as it had an inundation level of 0.46 km² (4.42%). For the sub-area NC4, the WW scenario was proven to be worthwhile. It showed 0 to 0.32 km² (0 to 2.07%) inundation for the arrival time (8 to 24 h). The main reason the WW scenario was the most suitable for the most areas was that it confined the flood within the channel. In contrast, the maximum inundation was observed for the WOWL scenario, which was about 12.41 km² (81.64%).

For NC5, the WL scenario was proven to be effective as it observed 0 to 0.75 km² (0 to 10.71%) inundation during all arrival times. However, the rest of the scenarios showed constant inundation ranging from 0.91 to 4.19 km² (i.e., 13–59.85%), with the maximum inundation observed in WWL scenarios. The WW scenarios showed a 0 to 0.56 km² (0 to 9.73%) inundation for the NC6 sub-area, which was the best scenario for saving the area from being flooded. Inundation in the sub-area NC7 should be prevented. The WW scenario proved to be an effective flood control measure as the inundation was only recorded up to 1.82 km² (30.33%). Amongst all the sub-areas, NC8 was the most flooded sub-area since it was the downstream sub-area. The area was inundated up to 10.82 km² (73.60%). Flooding in the area was mainly due to the impact of other structural measures in the upstream area, causing all the water to accumulate in NC8. None of the scenarios except WOWL were suitable to prevent flooding in this sub-area. Interestingly, for the sub-area NC10, the WL and WOWL scenarios were observed to be more effective as they held and delayed the flood water for up to 16 h. As time passed, the submerged area was recorded as being up to 8.58 km² (44.15%). It can be concluded that the WW scenarios would be more effective for the NC2, NC4, NC6, and NC10 sub-areas, which are bounded by urbanization, since they showed inundation levels of 3.21 km² (38.21%), 0.26 km² (1.71%), 0.46 km² (8%), and 3.32 km² (25%), respectively, whereas for the rest of the sub-areas, except NC8, the WL scenario can be considered a more effective flood retention approach. Figure 11 shows how all parts of the city would flood.

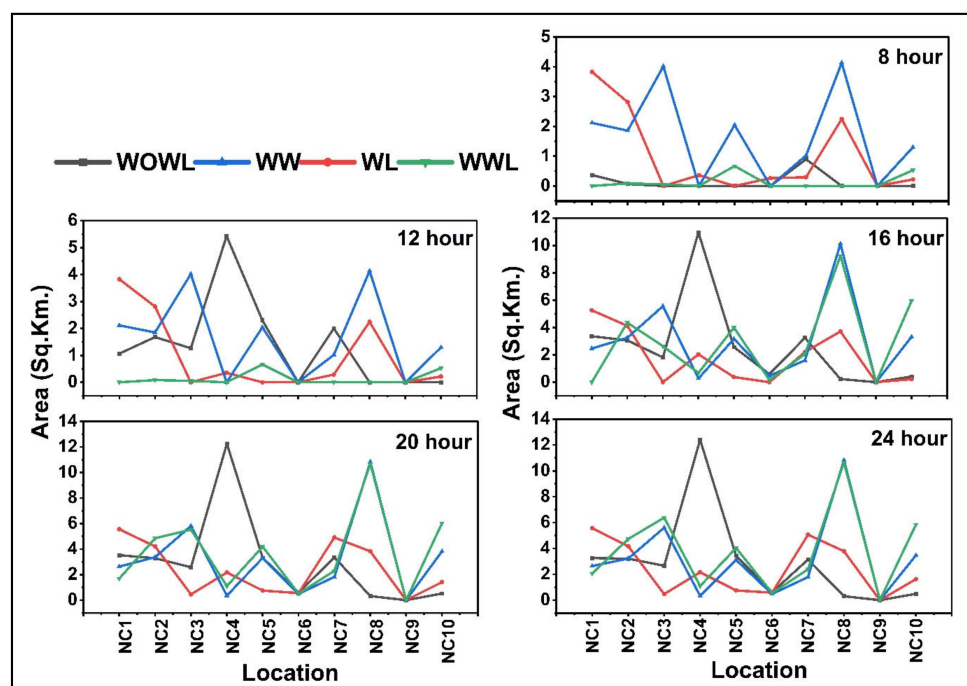


Figure 11. Submergence area profile along the Purna River for the 2004 flood.

4.1.3. Comparison of Error Analysis of Profiles for Four Scenarios

Computing the mean error was another method for determining which of the four scenarios had the best fit. The mean error showed how far the projected value of the flood depth (i.e., the simulated value) was from the observed value. In the current study, the mean error was calculated using WOWL as a standard case for each of the four scenarios. The profile that delivered the highest positive maximum error showed the flood level well below the typical situation (i.e., WOWL). A negative error showed that the flood depth was more than the expected value (i.e., WOWL). The scenario with the highest positive error among the four indicated the best flood retention response. Figure 12 shows the mean inaccuracy for all the scenarios as well as the arrival time (12, 16, 20, and 24 h). The two profiles (i.e., 1 and 2) were compared at the 12-h mark. Profile 1 was located on the right bank of the river and profile 2 was located on the left bank. A mean error was calculated by comparing the simulated water depths of the standard case (WOWL) and profile 1. Additionally, the average of all errors was calculated for each situation. The outcomes show that all errors for the 12th hour are positive, indicating that the predictions for all four scenarios for profiles 1 and 2 were understated. Therefore, for situations WW, WL, and WWL, the simulated depth was lower than the standard case (i.e., WOWL). In contrast to WL and WWL, which varied between 1.36 and 1.81 m for profile 1 and 1.78 m for profile 2, very little inaccuracy was observed in the WW scenario (i.e., for profile 1 it was 0.62 m, while for profile 2 it was 0.33 m). In comparison with the actual situation in the field, this was encouraging. The mean error for the WOWL comparison in the 16th hour was positive (i.e., for profiles 1 and 2 it was observed to be 2.16 and 2.69 m, respectively). However, for the WW scenario, a very small inaccuracy (positive) was noted (i.e., 0.13 m and 0.02 m for profiles 1 and 2). Additionally, for the WL and WWL scenarios, profile 1 showed negative errors (−0.71 and −0.88 m) whereas profile 2 showed positive errors (1.53 and 1.6 m). As was previously stated, the positive error showed that the water level in profile 1 was lower than the typical scenario (WOWL). As can be observed, the error for profile 2 in the WL and WWL scenarios is negative, indicating that this profile did outperform compared with the typical (WOWL) scenario. On the other hand, the WW scenario's inaccuracy was practically nil, indicating that it was holding back and postponing the flood. As a result, the most effective scenario for structural flood control measures was the WW scenario, which showed a very small inaccuracy. Because of the aforementioned structural flood retention features, the water depth was increased beyond the usual scenario. As a result, the error was negative, suggesting an ineffective scenario for the specific area in question.

In the case of WW scenarios, a negative error was observed for the 20th hour for both profiles 1 and 2 (−0.07 to −0.09 m). Profile 1 exhibited a negative error (−0.92 and −1 m) for WL and WWL scenarios, while profile 2 showed a positive error (0.49 and 0.35 m). Furthermore, with the exception of the WOWL cases for profiles 1 and 2, all other scenarios exhibited a negative error for the 24th hour. The errors for WL and WWL were the highest when compared with the WW scenarios, with (−0.78 and −0.87 m) for profile 1 and (−1 and −1.13 m) for profile 2, suggesting that the WW and WWL scenarios failed to manage or hold the flood since they surpassed the flooding in the WOWL case. It is therefore strongly recommended that WW was the most suitable scenario because the error was observed to be low or extremely low compared with the other scenarios for all arrival times. The best scenario for the design of structural flood retention measures was the WW scenario due to two strong reasons when compared to the lumped model system:

1. It delayed the flood's arrival time for almost 16 h.
2. It managed the flood better than the WOWL scenarios.

The mean error analysis of profiles 1 and 2 with respect to arrival times for all four scenarios is illustrated in Figure 12.

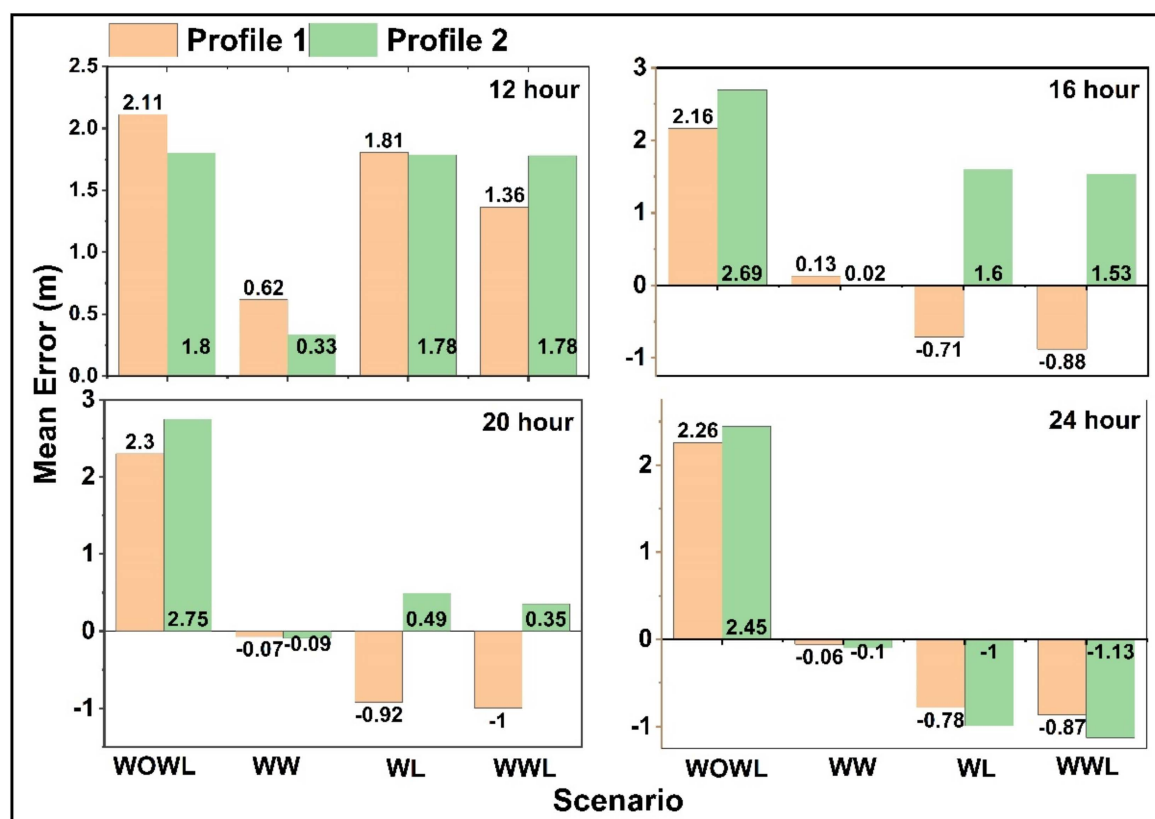


Figure 12. Error analysis of profiles 1 and 2 with respect to arrival time for all four scenarios.

4.2. Validation and Justification of the Model Based on Mesh Grid Stability and Its Impact on Flood Inundation

HEC-RAS 2D hydrodynamic modeling was used to generate the simulated flood inundation maps (Figure 13). Figure 14 shows a total of twelve observed water depth locations. The observed depth collected from the field survey was compared with the simulated water depth obtained from the HEC-RAS 2D models for different mesh grid structures (100×100 m, 90×90 m, and 50×50 m). In order to verify the consistency and performance of the models, a total of five statistical metrics (R^2 , RMSE, NSE, simulation time, and inundation area) were evaluated. Simulation results demonstrated that the effect of the different mesh grid structures on flood extent and inundation was significant. Furthermore, significant differences in computational time were observed.

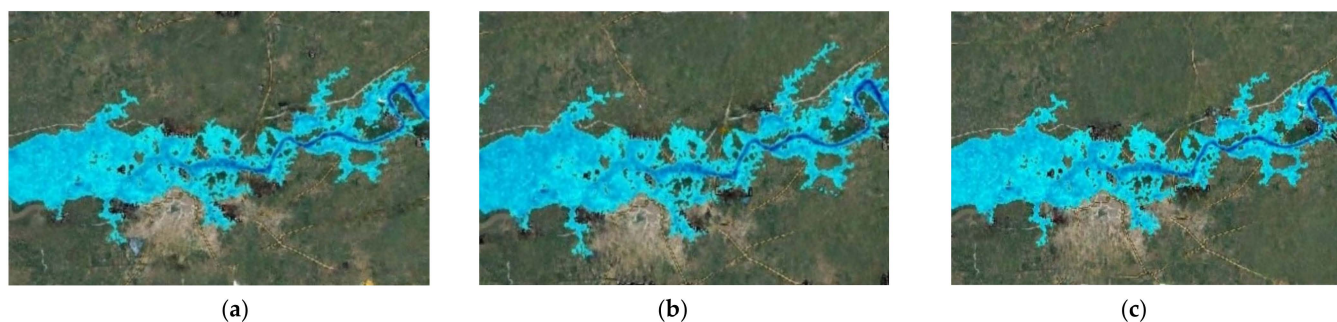


Figure 13. Flood inundation maps of the study area using varied mesh grid structures (a) 100×100 m, (b) 90×90 m, (c) 50×50 m.



Figure 14. A total of 12 observed water depth locations for the year 2004 (4 August).

Table 3 depicts the statistical analysis of the various mesh grid structures. Regression analysis of the simulated outcomes for different mesh structures revealed R^2 values ranging from 0.97 to 0.98. Given this, it is evident that mesh grid structures have a significant impact on flood inundation modeling. Three parameters were adjusted in each simulated result, viz. calculation time, prediction accuracy, and inundation area. Increasing the mesh size was found to increase the model's accuracy. The 50 m mesh grid structure model was more accurate than the 100 m and 90 m mesh grid models, with a high RMSE value of 0.53 (Refer Table 3). In contrast, the computing time for a 50 m mesh size was found to be significantly longer (i.e., 02 h: 25 m: 35 s) than for a 90 m mesh size (i.e., 02: 12 m: 43 s). Furthermore, the simulated inundation area for the 50 m mesh model was observed to be less (114 km^2) when compared with the 100 m and 90 m grid structure models (i.e., 118.66 and 122.96 km^2). In contrast, a shorter simulation time is associated with less accurate outcomes. This pertains to the very short simulation period for the 100 m and 90 m grid structure models (14 m: 15 s and 12 m: 08 s, respectively), resulting in quite substantial RMSE values of 0.57 and 0.56. Furthermore, the NSE value for the mesh size of 50 m^2 was 0.98, whilst the NSE values for the mesh sizes of 100 m and 90 m were 0.97 and 0.97, respectively. As a result, the 50 m mesh grid model outperforms other mesh grid structure models in terms of accuracy.

Table 3. Statistical parameters for comparison of diverse mesh grid structures.

Mesh Size m	R^2	RMSE m	NSE m	Computation Time (hh:mm:ss)	Inundation Area (km^2)
100×100	0.9785	0.567	0.971	00:14:15	118.66
90×90	0.9804	0.526	0.975	00:12:08	122.96
50×50	0.9855	0.450	0.982	02:25:35	114.61

5. Discussion

Flooding is a recurring phenomenon that causes financial losses and fatalities. Therefore, it is critical to respond to such floods in a way that minimizes harm to the environment, people, and infrastructure. In the past 20 years, several 2D hydrodynamic flood assessment studies have been conducted. In order to minimize the effects of the flood, researchers have proposed flood mitigation and management measures [32,39,40]. HEC-RAS 2D was used to create flood inundation maps for 10-, 20-, and 100-year flood events [29]. As the findings demonstrate, the mesh sizes of (25, 50, and 75 m) had no significant effect on performance. The simulation time, on the other hand, varied significantly. Azad et al. [30] investigated the sensitivity of a 2D shallow water model's unstructured mesh size, paying

special attention to mesh size and model functioning time in order to truly comprehend the model's accuracy and robustness. With diverse sized mesh structures, the HEC-RAS 2D was used on the urban floodplain of Kilicozu Creek in Kirsehir, Turkey. The impacts of land cover and topography on flood depth, arrival time, flow velocity, and extent were highlighted in the study. The results suggested that high-resolution land cover and very fine-resolution topography data may not be needed for HEC-RAS 2D modeling to produce reliable simulations [31].

The scenario-based stability of mesh grid structures in flood inundation and the integration of GIS with hydrodynamics, however, has not been heavily researched. Therefore, this study provides a novel technique for flood mitigation and the design of control measures consisting of a scenario-based flood retention plan coupled with the most realistic mesh grid model. The current study emphasizes the stability and impact of mesh grid structures on flood inundation based on scenario-based flood retention. The output of the model indicated that the inundation depth did not vary significantly, however, significant heterogeneity in the simulation time and flooding area was exhibited which has also been confirmed in several other studies [29–31].

The map depicting observed flood inundation was unavailable. Figure 15 depicts the real flood inundation map of Navsari city, which was constructed using the IDW interpolation tool in ArcGIS. Ideally, the IDW will safely presume that things that are close together are more similar than those that are further apart. The IDW predicts a value for any unmeasured region based on the observed values (flood depth) surrounding the prediction region. The measured values that are closer to the projected region influence the predicted value more than those that are further away. Table 4 depicts the results of the estimated areas inundated by floods in five intensity classifications (very low, low, moderate, high, and very high) for all sub-areas within the city of Navsari. The greatest flood coverage reported in sub-area NC9 within the 'very low' risk intensity class was 29.11% (2.11 km²). Maximum 'low' intensity flood coverage was observed for NC9, with 32.53 % of the total area inundated (3.14 km²). Furthermore, NC2 supplied the most land to the 'moderate' intensity class with 34.76 % (2.91 km²), followed by NC6 and NC10 with the next highest inundation coverage. Sub-area NC1 in the 'high' intensity class recorded the highest flood inundation coverage at 34.41 % (2.75 km²), followed by sub-areas NC10 and NC4 with the next highest coverage. In addition, sub-area NC7 under the 'very high' intensity class recorded the largest flooding area at 36.65% (2.21 km²), followed by sub-areas NC1 and NC6.

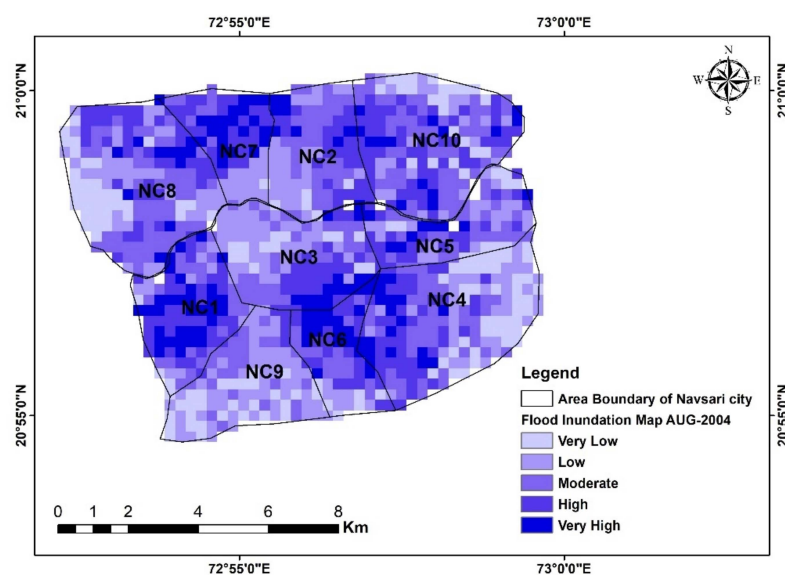


Figure 15. Observed flood inundation map of the Navsari city for the year 2004 (4 August) (Generated using GIS).

Table 4. Areal extent of flood inundation within 10 identified sub areas in Navsari City.

Class	Area	NC1	NC2	NC3	NC4	NC5	NC6	NC7	NC8	NC9	NC10
Very Low	km ²	1.02	1.39	2.01	3.90	1.70	0.86	0.39	3.82	2.81	2.31
	%	12.76	16.60	19.40	25.60	24.46	15.00	6.46	25.98	29.11	17.44
Low	km ²	0.20	1.07	2.41	2.13	1.17	0.00	0.42	0.76	3.14	1.16
	%	2.50	12.78	23.26	13.98	16.83	00	6.96	5.32	32.53	8.76
Moderate	km ²	1.53	2.91	1.85	3.44	1.64	1.72	1.43	4.39	2.07	3.91
	%	19.14	34.76	17.85	22.58	23.59	30.01	23.71	29.86	21.45	29.53
High	km ²	2.75	1.48	2.41	4.22	1.46	1.56	1.58	3.87	0.42	4.08
	%	34.41	17.68	23.26	27.70	21.00	27.22	26.20	26.32	4.35	30.81
Very High	km ²	2.49	1.52	1.68	1.54	0.98	1.59	2.21	1.86	1.21	1.78
	%	31.11	18.16	16.21	10.11	14.10	27.74	36.65	12.65	12.53	13.44

5.1. The Following Are the Benefits of the Proposed Flood Retention Plan

- Local disaster authorities can carry out the evacuation of people surrounding the city, reducing the loss of property and lives.
- Overall, vulnerability can be significantly reduced by employing the approach outlined in this study. Furthermore, the salinity of the water will rise, and the excess water can be utilized for irrigation since 40% of the Navsari city is agricultural land, which will result in increased revenue.
- Tide waves affect the city for approximately 23 km from the Arabian Sea (downstream) to Supa village (upstream) [32]. Because the Purna river is perennial, seawater intrusion is observed throughout the year. The effect of seawater will be significantly reduced by providing structural flood control measures.
- As a result, the city will have access to fresh water which is currently being pumped from the Ukai reservoir. Adopting flood retention measures in the study area could provide significant benefits to the city.
- Finally, the study's novel approach to flood retention measures can reveal scientific contributions in the context of flood management, mitigation, and resilience strategies.

5.2. The Following Are the Advantages of the HEC-RAS Model over the Other Models

- MIKE 21 is a commercial model, whereas HEC-RAS is open-source software. Mike 21 successfully accounts for inland application functions such as precipitation, evapotranspiration, flooding and drying, bottom shear stress, momentum dispersion, sources, and sinks; however, hydrological processes such as precipitation, infiltration, and evaporation of the river are expected to be minimal and ignored, even though the simulation in HEC-RAS may also be disrupted by silty clay soil and heavy rainfall [24]. MIKE21, also uses all the bathymetry data and requires a specific elevation value or land value to separate the floodplain from the overland. This method of dividing or fixing a flow area in 2D models differs from HEC-RAS, which uses a 2D flood area to fix the flow range. The flood visualization tools in HEC-RAS provide a more accurate representation of the flooding event than MIKE 21. The perceived differences in pre- and post-processing have made MIKE 21 a less appealing option. As a result of these drawbacks, HEC-RAS can be considered a preferable alternative [41,42].
- LISFLOOD-FP is an open-source raster-based 2D model built on the inertial formulation of the shallow-water equations by the University of Bristol [43]. HEC-RAS on the other hand, is popularly used for a wide range of applications such as 1D, 2D, and combined 1D–2D modeling, solving the implicit solution algorithm allowing for larger computational time steps than with explicit methods, unstructured and structural computation mesh, and mapping of the inundated area, as well as animations of the flooding which can be conducted inside of HEC-RAS using the RAS Mapper features. Furthermore, the newly released HEC-RAS model (HEC-RAS version 6.3.1) solves

either the 2D Shallow Water equations (with optional momentum additions for turbulence, wind forces, mud and debris flows, and Coriolis effects) or the 2D Diffusion Wave equations. HEC-RAS's ability to integrate the sub-grid bathymetry component has increased its resourcefulness in depicting topographical details by computing more samples of illuminating property tables for each cell face. The LISFLOOD model, on the other hand, uses the same high-resolution rectangular mesh as the input terrain raster. The mesh size had a significant impact on the LISFLOOD-FP output accuracy. When the inundation boundary was taken into account, the finer grid model outperformed the coarser grids. The ability of finer resolution models to capture more terrain details and route the flow in the correct direction while taking depressions and relief into account was one of the major reasons for the better performance, whereas the HEC-RAS model produced comparable results across resolutions and sub-grid terrain configurations [44,45].

- TELEMAC 2D is an open-source hydrodynamic model based on Saint-Venant equations. It uses a finite element scheme based on triangular elements, whereas the newly released HEC-RAS version 5.0 simulates 1D–2D modeling using a finite-volume scheme. Flood risk assessment and mapping results from HEC-RAS are more accurate than those from TELEMAC 2D because it is easy to simulate the model with different mesh sizes in HEC-RAS [46].
- ANUGA Hydro is an open-source hydrodynamic model. It solves shallow water equations, whereas HEC-RAS 2D solves shallow water equations and diffusion wave equations. Furthermore, HEC-RAS 2D uses an implicit finite volume algorithm. Although, ANUGA Hydro also uses a finite volume scheme. The ANUGA Hydro is designed to use a flexible mesh only [41]. In contrast, HEC-RAS is designed to use non-structural computational mesh. However, it is capable of handling structural mesh too [47–50].

5.3. The Following Are the Limitations and Recommendations of the Proposed Flood Retention Plan

- The present study does not examine the design considerations of flood control structures such as weirs, dams, and levees. If the dimensions pertaining to the hydraulic design (i.e., top width, bottom width, HFL, etc.) are assessed, the effect of flood control measures could be adequately addressed.
- In this analysis, neither the cost of flood control measures nor a cost-benefit analysis are taken into account.

6. Conclusions

Navsari city is located along the Arabian Sea coast and is prone to flooding during the monsoon season, resulting in large-scale human deaths and property losses. As a result, strong structural measures should be put in place to prevent disaster and mitigate damage. The most beneficial alternatives are structural measures in floodplains, but the cost of designing a flood retention plan is a major consideration. In this context, the current study proposed a novel approach for flood retention plans by using the HEC-RAS 2D hydrodynamic model to simulate four scenarios (i.e., WOWL, WW, WL, and WWL). The results showed that the 50 m mesh grid model produced more accurate results, with high NSE and R^2 values (0.98 and 0.98, respectively), a low RMSE value (0.45 m), and a smaller inundation area (114.61 km²). The results also revealed that, among the others, the WW scenario was an effective flood control measure as it held the flood water till the 16th hour arrival time and managed floods with WOWL scenarios. Following that, a comparison of flood depth, submergence area, and mean error was carried out to evaluate the models' adequacy, consistency, and efficacy. The WW case undoubtedly revealed accurate results, as the mean error for profiles 1 and 2 varied between (−0.7 to 0.62 m) and (−0.1 to 0.02 m), which were considered very low when compared with the other cases. However, the cost and availability of resources have been ignored in this study, which might be due to its

limited scope. Furthermore, a higher implicit scheme with effective tools can be used for the simulation of the same model, overcoming the shortcomings of HEC-RAS software. Using 2D HEC-RAS modeling, the novel approach of employing mesh grid impact assessment on flood inundation along with scenario-based structure flood retention plan (FRP) can be applied to any location around the world.

Author Contributions: Conceptualization, A.P., P.A., K.K., D.P. and S.S.; methodology, A.P. and P.A.; software, A.P.; validation, A.P., P.A. and S.K.S.; formal analysis, A.P., P.A., K.K., D.P. and S.S.; investigation, A.P. and P.A.; resources, A.P., P.A. and K.K.; writing—original draft preparation, A.P., P.A., S.S. and D.P.; writing—review and editing, A.P.; visualization, A.P. and P.A.; supervision, P.A.; funding acquisition. All authors have read and agreed to the published version of the manuscript.

Funding: This research received no external funding.

Institutional Review Board Statement: Not applicable.

Informed Consent Statement: Not applicable.

Data Availability Statement: The data that support the findings of this study are openly available in [USGS] at [<https://earthexplorer.usgs.gov>], accessed on 12 May 2019].

Acknowledgments: The authors would like to acknowledge anonymous reviewers for their useful comments and suggestions that have greatly enhanced the quality of this manuscript.

Conflicts of Interest: On behalf of all authors, the corresponding author states that there is no conflict of interest.

Abbreviations

HEC-RAS	Hydrologic Engineering Centre-River Analysis System
2D and 3D	Two and Three dimensional modeling
WOWL	Without Weir and Levees
WW	With Weir
WL	With Levees
WWL	With Weir and Levees
R ²	Coefficient of determination
RMSE	Root Mean Square Error
NSE	Nash Sutcliffe Efficiency
DEM	Digital Elevation Model

References

1. Patel, D.P.; Srivastava, P.K. Flood Hazards Mitigation Analysis Using Remote Sensing and GIS: Correspondence with Town Planning Scheme. *Water Resour. Manag.* **2013**, *27*, 2353–2368. [[CrossRef](#)]
2. Khattak, M.S.; Anwar, F.; Saeed, T.U.; Sharif, M.; Sheraz, K.; Ahmed, A. Floodplain Mapping Using HEC-RAS and ArcGIS: A Case Study of Kabul River. *Arab. J. Sci. Eng.* **2015**, *41*, 1375–1390. [[CrossRef](#)]
3. Patel, D.P.; Dholakia, M.B. Feasible structural and non-structural measures to minimize effect of flood in Lower Tapi Basin. *Wseas Trans. Fluid Mech.* **2010**, *3*, 104–121.
4. Sahoo, S.N.; Sreeja, P. Development of Flood Inundation Maps and Quantification of Flood Risk in an Urban Catchment of Brahmaputra River. *Asce-Asme J. Risk Uncertain. Eng. Syst. Part A Civ. Eng.* **2017**, *3*, A4015001. [[CrossRef](#)]
5. Shao, Z.; Jahangir, Z.; Muhammad Yasir, Q.; Mahmood, S. Identification of Potential Sites for a Multi-Purpose Dam Using a Dam Suitability Stream Model. *Water* **2020**, *12*, 3249. [[CrossRef](#)]
6. Vermuyten, E.; Van Uytven, E.; Meert, P.; Wolfs, V.; Willems, P. Real-Time River Flood Control under Historical and Future Climatic Conditions: Flanders Case Study. *J. Water Resour. Plan. Manag.* **2020**, *146*, 05019022. [[CrossRef](#)]
7. Pathan, A.I.; Agnihotri, P.G. Application of new HEC-RAS version 5 for 1D hydrodynamic flood modeling with special reference through geospatial techniques: A case of River Purna at Navsari, Gujarat, India. *Model. Earth Syst. Environ.* **2020**, *7*, 1133–1144. [[CrossRef](#)]
8. Singh, O.; Kumar, M. Flood occurrences, damages, and management challenges in India: A geographical perspective. *Arab. J. Geosci.* **2017**, *10*, 102. [[CrossRef](#)]
9. Roux, H.; Dartus, D. Sensitivity Analysis and Predictive Uncertainty Using Inundation Observations for Parameter Estimation in Open-Channel Inverse Problem. *J. Hydraul. Eng.* **2008**, *134*, 541–549. [[CrossRef](#)]

10. Abdella, K.; Mekuanent, F. Application of hydrodynamic models for designing structural measures for river flood mitigation: The case of Kulfo River in southern Ethiopia. *Model. Earth Syst. Environ.* **2021**, *7*, 2779–2791. [\[CrossRef\]](#)
11. Ranzi, R.; Mazzoleni, M.; Milanesi, L.; Pilotti, M. *Critical Review of Non-Structural Measures for Water-Related Risks*; KULTURisk: Delft, The Netherlands, 2011; p. 42.
12. Tanim, A.H.; Goharian, E. Developing a hybrid modeling and multivariate analysis framework for storm surge and runoff interactions in urban coastal flooding. *J. Hydrol.* **2020**, *595*, 125670. [\[CrossRef\]](#)
13. Liao, K.-H. A Theory on Urban Resilience to Floods—A Basis for Alternative Planning Practices. *Ecol. Soc.* **2012**, *17*, 15. [\[CrossRef\]](#)
14. Zhixiong, D.; Yalin, H.; Jiren, L.; Shifeng, H. A Model of Flood and Waterlogging Disaster Loss Assessment Based on The Remote Sensing and GIS Spatial Information Grid. Impacts of Global Climate Change. 2005, pp. 1–8. Available online: <https://ascelibrary.org/doi/10.1061/40792%28173%29136> (accessed on 30 October 2022). [\[CrossRef\]](#)
15. Skalak, K.J.; Benthem, A.J.; Schenk, E.R.; Hupp, C.R.; Galloway, J.M.; Nustad, R.A.; Wiche, G.J. Large dams and alluvial rivers in the Anthropocene: The impacts of the Garrison and Oahe Dams on the Upper Missouri River. *Anthropocene* **2013**, *2*, 51–64. [\[CrossRef\]](#)
16. Bala, S.K.; Islam, A.S.; Chowdhury, J.U.; Rahman, M.R.; Haque, M.A.; Khan, M.S.A.; Salehin, M. Performance of flood control works around Dhaka city during major floods in Bangladesh. In *Proceedings of the Second International Conference on Water and Flood Management*; Institute of Water and Flood Management: Dhaka, Bangladesh, 2009; pp. 1–10.
17. Obi Lawrence, E. Application of retaining wall in the control of flooding and gully erosion. *Am. J. Eng. Res.* **2017**, *6*, 203–206.
18. Gotoh, H.; Maeno, Y.; Takezawa, M.; Ohnishi, M. Flood control and small-scale reservoirs. *River Basin Manag.* **2011**, *146*, 51–60. [\[CrossRef\]](#)
19. Jayswal, A.R.; Malekwala, F.S.; Rautela, C. Flood protection work by Terramesh wall. *Int. J. Sci. Res. Dev.* **2014**, *2*, 2321–0613.
20. Quirogaa, V.M.; Kurea, S.; Udoa, K.; Manoa, A. Application of 2D numerical simulation for the analysis of the February 2014 Bolivian Amazonia flood: Application of the new HEC-RAS version 5. *Ribagua* **2016**, *3*, 25–33. [\[CrossRef\]](#)
21. Azeez, O.; Elfeki, A.; Kamis, A.S.; Chaabani, A. Dam break analysis and flood disaster simulation in arid urban environment: The Um Al-Khair dam case study, Jeddah, Saudi Arabia. *Nat. Hazards* **2019**, *100*, 995–1011. [\[CrossRef\]](#)
22. USACE. HEC-RAS River Analysis System Hydraulic Reference Manual. Hydrologic Engineering Center 547. 2016. Available online: <https://www.hec.usace.army.mil/software/hec-ras/documentation/HEC-RAS%205.0%20Reference%20Manual.pdf> (accessed on 15 January 2022).
23. Zhang, L.; Xu, Y.; Liu, Y.; Peng, M. Assessment of flood risks in Pearl River Delta due to levee breaching. *Georisk Assess. Manag. Risk Eng. Syst. Geohazards* **2013**, *7*, 122–133. [\[CrossRef\]](#)
24. Patel, D.P.; Ramirez, J.A.; Srivastava, P.K.; Bray, M.; Han, D. Assessment of flood inundation mapping of Surat city by coupled 1D/2D hydrodynamic modeling: A case application of the new HEC-RAS 5. *Nat. Hazards* **2017**, *89*, 93–130. [\[CrossRef\]](#)
25. Fadillah, R.M.; Tsaqib, H.; Nurendyastuti, A.K.; Jannah, M.; Prastica, R.M.S. Structural mitigation measures for flood reduction in urban area: A case study of Ciliwung watershed. In *E3S Web of Conferences*; EDP Sciences: Les Ulis, France, 2020; Volume 200, p. 01004.
26. Cherinet, A.; Worku, S. Flood Inundation Mapping of Jigjiga-Town and Its Surrounding Environment: Using GIS & HEC-RAS Model. *Int. J. Environ. Prot. Policy* **2021**, *9*, 40. [\[CrossRef\]](#)
27. Fadilah, S.; Istiarto; Legono, D. Investigation and modelling of the flood control system in the Aerotropolis of Yogyakarta International Airport. *IOP Conf. Ser. Mater. Sci. Eng.* **2021**, *1173*, 012015. [\[CrossRef\]](#)
28. Motlagh MB, Hassanpour F, Tabatabaei SM Flood management of Sistan river using levee. *J. Acad. Appl. Stud.* **2013**, *3*, 32–45.
29. Ongdas, N.; Akiyanova, F.; Karakulov, Y.; Muratbayeva, A.; Zinabdin, N. Application of HEC-RAS (2D) for Flood Hazard Maps Generation for Yesil (Ishim) River in Kazakhstan. *Water* **2020**, *12*, 2672. [\[CrossRef\]](#)
30. Azad, W.H.; MohdSidek, L.; Basri, H.; Hassan, A.J. Dissimilarity mesh size assessment for two di-mensional flood routing model. In *International Conference on Dam Safety Management and Engineering*; Springer: Singapore, 2019; pp. 245–255.
31. Yalcin, E. Assessing the impact of topography and land cover data resolutions on two-dimensional HEC-RAS hydrodynamic model simulations for urban flood hazard analysis. *Nat. Hazards* **2020**, *101*, 995–1017. [\[CrossRef\]](#)
32. Pathan, A.I.; Agnihotri, P.G.; Patel, D.; Prieto, C. Identifying the efficacy of tidal waves on flood assessment study—A case of coastal urban flooding. *Arab. J. Geosci.* **2021**, *14*, 2132. [\[CrossRef\]](#)
33. Huang, W.; Zhang, H.; Zhu, L.; Chen, L.; Zhang, G.; Gong, W.; Liu, J. In-situ study of the spatiotemporal variability of sediment erodibility in a microtidal estuary. *Estuar. Coast. Shelf Sci.* **2020**, *232*, 106530. [\[CrossRef\]](#)
34. Zhou, Z.; Liu, S.; Zhong, G.; Cai, Y. Flood Disaster and Flood Control Measurements in Shanghai. *Nat. Hazards Rev.* **2017**, *18*, B5016001. [\[CrossRef\]](#)
35. Brunner, G.W. *HEC-RAS River Analysis System, 2D Hydraulic Reference Manual, Version 5.0*; Hydrologic Engineering Center: Davis, CA, USA, 2016.
36. Kim, B.; Sanders, B.F.; Schubert, J.E.; Famiglietti, J.S. Mesh type tradeoffs in 2D hydrodynamic modeling of flooding with a Godunov-based flow solver. *Adv. Water Resour.* **2014**, *68*, 42–61. [\[CrossRef\]](#)
37. Chow, V. *Open Channel Hydraulics*; McGraw-Hill: New York, NY, USA, 1959.
38. Chow, V.; Maidment, D.; Mays, L. Design Storms. Applied Hydrology. 1988. Available online: http://ponce.sdsu.edu/Applied_Hydrology_Chow_1988.pdf (accessed on 18 February 2022).

39. Patel, D.; Srivastava, P.; Singh, S.K.; Prieto, C.; Han, D. Preparation of EAP for Ukai Dam using 1D/2D coupled hydrodynamic modelling and Google Earth image. In Proceedings of the International Dam Safety Conference, Thiruvananthapuram, India, 23–24 January 2018.
40. Faudzi, S.M.M. Two-dimensional simulation of sultan Abu Bakar dam release using HEC-RAS. *Int. J. Geomate* **2019**, *16*, 124–131. [[CrossRef](#)]
41. Teng, J.; Jakeman, A.J.; Vaze, J.; Croke, B.F.W.; Dutta, D.; Kim, S. Flood inundation modelling: A review of methods, recent advances and uncertainty analysis. *Environ. Model. Softw.* **2017**, *90*, 201–216. [[CrossRef](#)]
42. Shrestha, A.; Bhattacharjee, L.; Baral, S.; Thakur, B.; Joshi, N.; Kalra, A.; Gupta, R. Understanding suitability of MIKE 21 and HEC-RAS for 2D floodplain modeling. In *World Environmental and Water Resources Congress 2020: Hydraulics, Waterways, and Water Distribution Systems Analysis*; American Society of Civil Engineers: Reston, VA, USA, 2020; pp. 237–253. [[CrossRef](#)]
43. Bates, P.D.; Dawson, R.J.; Hall, J.W.; Horritt, M.S.; Nicholls, R.J.; Wicks, J.; Hassan, M.A.A.M. Simplified two-dimensional numerical modelling of coastal flooding and example applications. *Coast. Eng.* **2005**, *52*, 793–810. [[CrossRef](#)]
44. Shustikova, I.; Domeneghetti, A.; Neal, J.C.; Bates, P.; Castellarin, A. Comparing 2D capabilities of HEC-RAS and LISFLOOD-FP on complex topography. *Hydrol. Sci. J.* **2019**, *64*, 1769–1782. [[CrossRef](#)]
45. Stephens, E.; Bates, P.; Freer, J.; Mason, D. The impact of uncertainty in satellite data on the assessment of flood inundation models. *J. Hydrol.* **2011**, *414–415*, 162–173. [[CrossRef](#)]
46. EzzahraMaatar, F.; Domeneghetti, A.; Brath, A. HEC-RAS 5.0 vs. TELEMAC-2D: A Model Comparison for Flood-Hazard and Flood-Risk Estimation. EGU General Assembly Conference Abstracts. 2015, p. 910. Available online: <https://ui.adsabs.harvard.edu/abs/2015EGUGA..17..910E/abstract> (accessed on 30 October 2022).
47. Kantamaneni, K.; Rani, N.S.; Rice, L.; Sur, K.; Thayaparan, M.; Kulatunga, U.; Rege, R.; Yenneti, K.; Campos, L.C. A Systematic Review of Coastal Vulnerability Assessment Studies along Andhra Pradesh, India: A Critical Evaluation of Data Gathering, Risk Levels and Mitigation Strategies. *Water* **2019**, *11*, 393. [[CrossRef](#)]
48. Pathan, A.I.; Agnihotri, P.G.; Patel, D. Integrated approach of AHP and TOPSIS (MCDM) techniques with GIS for dam site suitability mapping: A case study of Navsari City, Gujarat, India. *Environ. Earth Sci.* **2022**, *81*, 443. [[CrossRef](#)]
49. Kantamaneni, K. Coastal infrastructure vulnerability: An integrated assessment model. *Nat. Hazards* **2016**, *84*, 139–154. [[CrossRef](#)]
50. Pathan, A.I.; Girish Agnihotri, P.; Said, S.; Patel, D. AHP and TOPSIS based flood risk assessment-a case study of the Navsari City, Gujarat, India. *Environ. Monit. Assess.* **2022**, *194*, 509. [[CrossRef](#)]